NANO · MICRO
small
www.small-journal.com

Layer-by-Layer Assembly of Strong Thin Films with High Lithium Ion Conductance for Batteries and Beyond

Zhen Wang, Liangqi Ouyang, Hailong Li, Lars Wågberg, and Mahiar Max Hamedi**

Polyethylene oxide (PEO) is one of the most widely used polymeric ion conductors which has the potential for a wide range of applications in energy storage. The enhancement of ionic conductivity of PEO-based electrolytes is generally achieved by sacrificing the mechanical properties. Using layer-by-layer (LbL) self-assembly with a nanoscale precision, mechanically strong and self-healable PEO/polyacrylic acid composite thin films with a high Li^+ conductivity of $2.3 \pm 0.8 \times 10^{-4}$ S cm^{-1} at 30 °C, and a strength of 3.7 MPa is prepared. These values make the LbL composite among the best recorded multifunctional solid electrolytes. The electrolyte thin film withstands at least 1000 cycles of striping/plating of Li at 0.05 mA cm^{-2}. It is further shown that the LbL thin films can be used as separators for Li-ion batteries to deliver a capacity of 116 mAh g^{-1} at 0.1 C in an all-LbL-assembled lithium iron phosphate/lithium titanate battery. Finally, it is demonstrated that the thin films can be used as ion-conducting substrates for flexible electrochemical devices, including micro supercapacitors and electrochemical transistors.

1. Introduction

Polyethylene oxide (PEO), also referred to as polyethylene glycol (PEG) with molecular weight less than 20 000 Da, is one of the most widely used polymeric ion conductors, and has been used for applications in energy storage and conversion.[1] The PEO chain can host Li^+ as well as many other ions and transport these ions via segment movement.[2] Pristine PEO, with a molecular weight higher than ≈600 g mol^{-1}, crystallizes at room temperature, and therefore its segment movement is hindered under a melting point of ≈65 °C, which limits the ionic conductivity of PEO-based electrolytes at ambient temperature.[3] To widen the range of working temperature for PEO based gel electrolytes toward room temperature, efforts have been made to incorporate plasticizers to suppress the crystallinity and thus enhance the PEO segment mobility. This approach, however, mostly results in materials with poor mechanical properties.[4]

Thin-film gel electrolytes not only support ion transport but can also act as the separator between electrodes in energy storage devices. The mechanical property of such electrolyte is therefore essential to the device performance.[4] A mechanically robust film can greatly reduce the minimum thickness required for the structural integrity.[5] Such a thin separator enables energy storage devices to pursue both high volumetric energy density and high power density. Up to date, the thickness of most PEO-based gel electrolytes are in the range of 50–500 µm,[6] significantly thicker than the standard porous polyethylene (PE) separator (≈20 µm) used in Li^+ ion batteries. The ionic conductivity of PEO-based solid-state electrolytes are typically in the range of 10^{-8} to 10^{-4} S cm^{-1} at room temperature,[3] which is lower than that of liquid electrolytes for Li^+ ion batteries, ranging from 10^{-3} to 10^{-2} S cm^{-1}.[7] For aqueous systems, for example, supercapacitors, the conductivity of the gel electrolytes reaches the order of 10^{-2} S cm^{-1}.[8] The preparation of thin but strong PEO-based electrolytes with high ionic conductivity still remains a challenge.

Layer-by-layer (LbL) self-assembly, allowing nanoscale self-assembly precision, is a promising approach to building PEO-based Li^+ conducting thin films with plasticizers/fillers incorporated as the technique naturally requires a minimal of two different compounds.[9] DeLongchamp et al. demonstrated PEO/polyacrylic acid (PAA) multilayers with Li^+ conductivity up to 2.3×10^{-5} S cm^{-1} at 52% RH,[10] and also showed that the thin film of PEO/PAA could be free-standing and exhibited elastomer-like mechanical property.[11] They also reported a polymer-clay structure from poly(ethyleneimine), Laponite clay, and poly(ethylene oxide) using, what they claimed to be, a combination of hydrogen bonding and electrostatic interactions, delivering an ionic conductivity of 4×10^{-8} S cm^{-1} at 53% relative humidity, for Li^+. Nguyen et al. prepared a solid polymer electrolyte film with an ionic conductivity of 9.1×10^{-4} S cm^{-1} at 90% RH using LbL assembly of polyethyleneimine (PEI)/PAA/PEO/PAA for electrochromic devices.[12] Nevertheless, none of

Dr. Z. Wang, Dr. L. Ouyang, Dr. H. Li, Prof. L. Wågberg,
Dr. M. M. Hamedi
Division of Fibre Technology
Department of Fibre and Polymer Technology
KTH Royal Institute of Technology
Teknikringen 56, Stockholm 10044, Sweden
E-mail: zhenwang@kth.se; mahiar@kth.se

Prof. L. Wågberg, Dr. M. M. Hamedi
Wallenberg Wood Science Centre
Department of Fibre and Polymer Technology
KTH Royal Institute of Technology
Teknikringen 56, Stockholm 10044, Sweden

The ORCID identification number(s) for the author(s) of this article can be found under https://doi.org/10.1002/smll.202100954.

DOI: 10.1002/smll.202100954

those previous reports demonstrated practical applications in Li-ion batteries where the ionic conductivity in the highly dry state should be higher than 10^{-4} S cm^{-1}.[13]

Here we employ an LbL assembly method from aqueous solutions to build dual cross-linked amorphous PEO/PAA electrolyte via non-ionic interactions, followed by heat-induced covalent bonding between the terminal groups of PEO and the carboxyl groups of PAA. We can obtain robust, self-healing, and free-standing PEO/PAA thin films, taking advantage of the nanoscale assembly precision. With water or the commonly used organic solvent of liquid electrolyte as the plasticizers, our PEO/PAA solid-state electrolyte shows a high ionic conductivity in both aqueous and organic systems. We demonstrate the application of the thin film solid-state electrolytes for Li-ion batteries, supercapacitor, and electrochromic devices.

2. Results and Discussion

2.1. The Build-Up of PEO/PAA Thin Films

At pH 2.4 where the carboxyl groups of PAA are protonated, PEO and PAA form a complex during the LbL assembly process which is entropically driven due to the release of trapped water molecules.[14] Once the films are formed the polymers are most probably able to form dynamic H-bonds as schematically shown in **Figure 1**a. Here each polymer layer overcompensated the available active sites from the previous layer, resulting in a reversed surface functionality that allows adsorption for the next layer, which enabled a continuous lay-by-layer growth with precise blending down to the molecular size level.[11]

It has also been established that the growth of the multilayers highly depends on the molecular weight of the polymers.[15] We employed quartz crystal microbalance with dissipation monitoring (QCM-D) to study the build-up of the multilayers composed of PEO and PAA of different molecular weights assigned as $(\text{PEO/PAAXX})_n$, where XX denotes the molecular weight of the polymer and n denotes the number of bilayers. As shown in Figure 1b and Figure S1, Supporting Information, PEO/PAA1.2k and PEO/PAA8k showed a low increase in mass with each layer and the layers grew linearly with the number of bilayers. For higher molecular weight of PAA, both PEO/PAA50k and PEO/PAA240k showed a much larger increase in mass per layer in a super-linear manner. After the build-up of the first 10 bilayers, the assembly of PEO and PAA240k showed a significant and steady LbL growth, which is shown in Figure 1c, and the formed $(\text{PEO/PAA240k})_{30}$ composite layer had a thickness of 5.1 µm in the dry state corresponding to an average thickness increase of 170 nm per bilayer. Tuning the assembly behavior with PAA of different molecular weights, we are able to tailor the precision of the average increase in thickness down to an impressive 3 nm per bilayer in $(\text{PEO/PAA1.2k})_{80}$.

Upon heat treatment, the complex PEO/PAA thin film formed covalent cross-links in addition to the possible H-bonding interaction (Figure 1a). The absorbance at 1760 and 1801 cm^{-1} in the FT-IR spectra (Figure S2a,b, Supporting Information) indicates the presence of anhydride. Further, anhydride can react with the terminal amino groups of PEO and form amide crosslinks during the heat treatment, which is indicated by the stability of the thin film after treating in an acid solution at 80 °C (Figure S2c,d, Supporting Information). These covalent bonds stabilized the film which stayed intact even after being soaked for 7 days in water of neutral pH (Figure S3, Supporting Information) where H-bonds would have been interrupted due to the disassociation of protons from the polymer chain of PAA.

The molecular level complex was assembled with excellent uniformity. The homogeneous PEO/PAA240k film had good transparency with an average transmittance of 89% in the visible light range (380–780 nm, Figure 1d). The surface and the cross-section of the $(\text{PEO/PAA240k})_{30}$ film shown in Figure 1e,f are smooth and dense. Atomic force microscopy (AFM) height image of the film surface (Figure 1g) shows an ultra-low root mean square roughness, Rq, of 0.3 nm over an area of 3 µm × 3 µm. We found no phase separation in Figure 1h, which indicates that a homogeneous composite structure is enabled by the highly precise LbL assembly technique.

2.2. Thermal and Mechanical Properties

Due to the incorporation of PAA, the segment mobility of PEO was partially hindered by the H-bonds which prevented the thermally driven chain rearrangement of PEO to form crystal domains. This is supported by the DSC heating curves in **Figure 2**a where no endothermic peak from the melting of PEO crystalline phase was observed for the $(\text{PEO/PAA240k})_{30}$ film. The DSC cooling curve in Figure S4a, Supporting Information also indicates that only PEO shows a crystalline peak at 41 °C and the $(\text{PEO/PAA240k})_{30}$ film was amorphous. The X-ray powder diffraction (XRD) patterns in Figure S4b, Supporting Information shows the $(\text{PEO/PAA240k})_{30}$ film lost the crystalline phase of PEO due to the nanoscale LbL assembly, which is in consistence with the DSC analysis. We measured a glass transition temperature (T_g) of 40 °C, which is between the T_g for pure PEO (−53 °C) and for pure PAA (96 °C). The single T_g indicated a homogeneous blending of the two polymer phases which is in consistence with AFM images in Figure 1h.

The cross-linked and homogeneously textured film was amorphous and showed elastomer-like mechanical properties, in being both strong and flexible. This property allowed the thin films to be peeled off from the polypropylene (PP) substrates and act as free-standing films. As shown in Figure 2b, at a relative humidity of 50% where moisture can be absorbed as a plasticizer, $(\text{PEO/PAA240k})_{30}$ showed robust mechanical properties with a strength of 3.0 ± 0.6 MPa and an elongation of 324 ± 30%. The interactions within the films also allowed for self-healing after cutting. As shown in Figure 2b,c, by overlapping the two edges together with an ultra-thin contact region of 60 µm margin, the $(\text{PEO/PAA240k})_{30}$ film were self-healed and showed similar mechanical behavior as the pristine samples. While being plasticized by propylene carbonate (PC), the $(\text{PEO/PAA240k})_{30}$ film showed a breaking strength of 3.7 ± 0.2 MPa and a breaking elongation of 311 ± 60%. In comparison, pure PEO dissolved after one day's soaking in 1 M LiTFSI in PC (Figure S5, Supporting Information).The strong mechanical properties promised the $(\text{PEO/PAA240k})_{30}$ thin film as a resilient separator for aqueous or organic electrolytes.

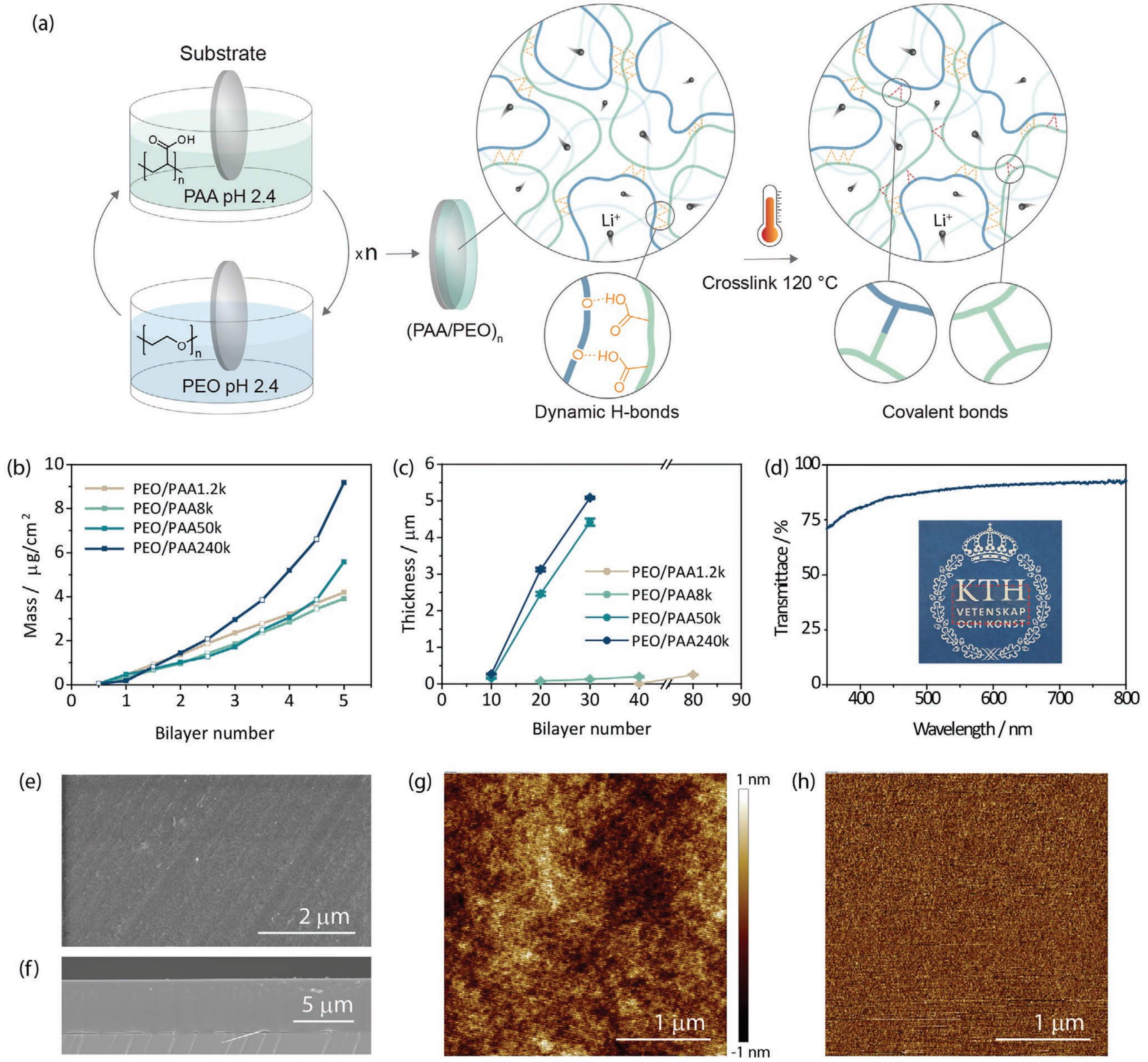

Figure 1. a) Schematic illustration of the process of LbL self-assembly and the heat-induced crosslinking. b) Mass growth calculated from the QCM data of the first five bilayers of PEO and PAA with various molecular weights. c) The thickness of the PEO/PAA films assembled with PAA of different molecular weights. d) Transmittance spectrum of the (PEO/PAA240k)$_{100}$. Inset is a photo of the corresponding sample with the shape indicated by the red dash line. Representative e) top-view SEM image, f) cross-sectional SEM images, g) height image from AFM, and h) peak force error image from AFM of the (PEO/PAA240)$_{30}$ composite thin film.

2.3. Ionic Conductivity

The cross-linked thin films could be swollen by water or organic solvents to enable incorporation of ions into the film through diffusion. We showed the LbL thin films could be used as solid-state gel electrolytes, using organic solvents as the plasticizer and ion carrier, for example PC and EC/DEC.

We introduced Li$^+$ into the network of PEO/PAA240k thin film where it could be transported by the segment movement of PEO. We found a nonlinear dependency of ionic conductivity on temperature, as shown in the Arrhenius plot in Figure 2d and Figure S6, Supporting Information. We fitted the ionic conductivity of the amorphous electrolyte to the Vogel–Tammann–Fulcher (VTF) model[16] with the equation:

$$\sigma = A\, e^{-E_a/R(T-T_0)} \qquad (1)$$

where σ is the ionic conductivity, A the prefactor, E_a the activation energy, R the gas constant, T the temperature, and T_0 the Vogel temperature. This show a nonlinear dependency which is indicative of a solid-state ionic conducting mechanism.[17] The ionic conductivity of PEO/PAA240k was $2.3 \pm 0.8 \times 10^{-4}$ S cm^{-1}

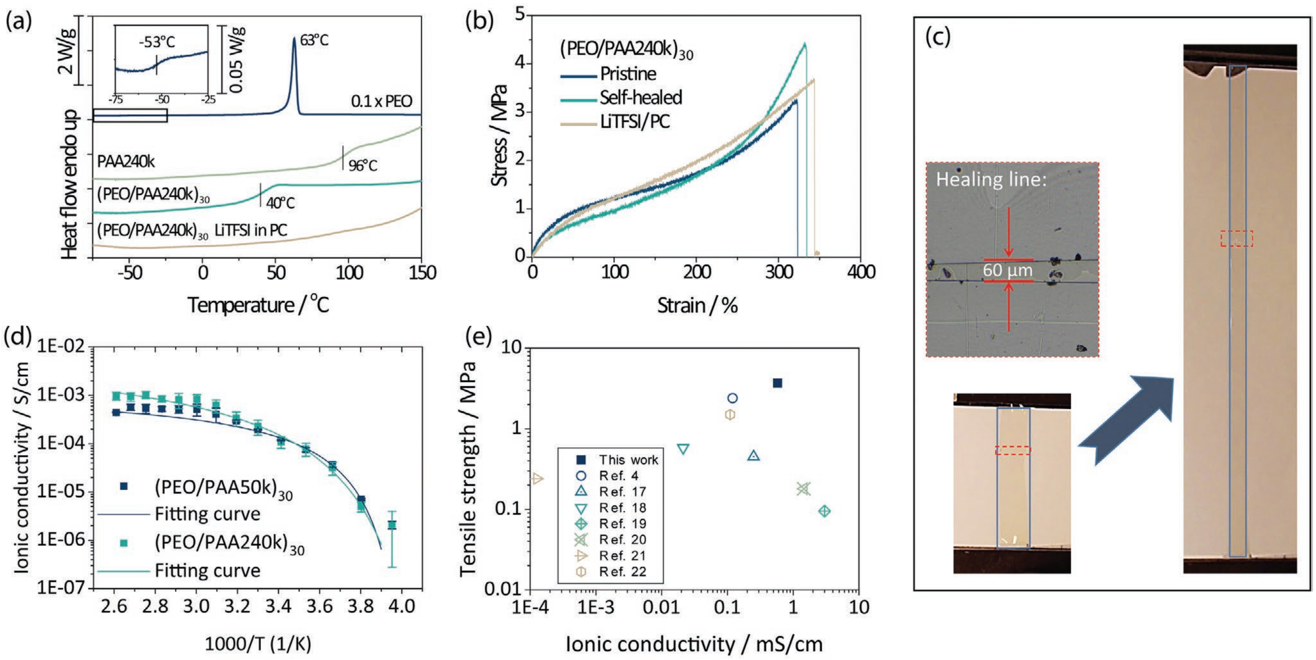

Figure 2. a) DSC curves the PEO/PAA films; b) stress–strain curves of the pristine, self-healed, and 1 M LiTFSI in PC soaked PEO/PAA films; c) photos showing the self-healed PEO/PAA film being stretched; d) lithium ion conductivity at different temperature of the PEO/PAA films soaked by 1 M $LiPF_6$ in EC/DEC (50/50 v/v). Curves fitted using the VTF model; e) comparison of ionic conductivity versus strength with previous reports.

at 30 °C, which is amongst the highest Li^+ conductivities reported for all polymeric gel electrolytes (Figure 2e),[4,17–22] while at the same time having a strength of 3.7 MPa. These values combined place our LbL composite among the best recorded multifunctional solid electrolytes.

2.4. Solid-State Electrolyte for LIB

Taking advantage of the ionic conductivity and the good stability, we evaluated the performance of the PEO/PAA thin-film soaked by 1 M $LiPF_6$ in EC/DEC as a solid-state electrolyte for lithium-ion batteries at room temperature. Benefitting from the mechanical robustness, the PEO/PAA240k thin film showed good stability in the cyclic plating/stripping test for at least 1000 h (1000 cycles) at a constant current of 0.05 mA cm^{-2} (**Figure 3**a,b). We found no battery short circuit during the cycling, which suggests that the separator is robust enough to suppress the growth of Li dendrites. We used cyclic voltammetry (CV) to study the half-cells assembled with the lithium titanate (LTO) anode and the lithium iron phosphate (LFP) cathode, respectively. As shown in Figure S7, Supporting Information, typical Li^+ insertion peaks are found with a current density of 50.3 mA g^{-1} at 1.3 V for LTO anode and 70.6 LFP at 3.7 V for LFP cathode and extraction peaks of 50.3 LFP at 1.8 V for LTO anode and 63.1 LFP at 3.2 V for LFP cathode at their corresponding potential window.

We evaluated the charge/discharge performance of the LTO anode. As shown in Figure S8, Supporting Information, the anode delivered a specific capacity of 79 mAh g^{-1} at 0.1 C and 14 mAh g^{-1} at 1 C. The capacities were believed to be limited by the relatively low Li^+ transference number. Nevertheless, the cyclic stability of the LTO anode was good with no capacity fading observed when charging/discharging at 1 C for 100 cycles with the Columbic efficiency higher than 99.4%.

2.5. LbL Self-Assembled LIB Anodes and Cathodes

We have recently shown that the LbL technique can be used for the build-up of LIB anodes and cathodes.[23] Here we combined these methods to LbL-assemble a full-cell LIB by attaching the PEO/PAA layers on top of LbL assembled anode and cathode, as schematically shown in Figure 3c. The scanning electron microscopic (SEM) images in Figure 3d,e show that the LbL assembled electrodes were embedded with good contact to the PEO/PAA thin film. Figure 3f shows that the full battery had typical charge/discharge profiles with a stable discharge voltage plateau at 1.8 V and a high specific capacity of 116 mAh g^{-1} at 0.1 C. The full battery showed good rate capability and could be stably charged/discharged at a current density up to 5 C. The full LIB started to stabilize after cycling 30 times at 1 C and showed slight performance fading in the last 470 cycles (Figure 3g). Though the capacity of the full LIB might be limited, the Columbic efficiency of the last 450 cycles was all higher than 99%.

2.6. Transparent, Free-Standing Ion Membrane for Electronic Devices

As shown in **Figure 4**a, the aqueous gel electrolytes delivered an ionic conductivity 0.33 ± 0.04 mS cm^{-1} for 1 M NaCl, 0.40 ± 0.04 mS cm^{-1} for 1 M KCl, 0.40 ± 0.06 mS cm^{-1} for

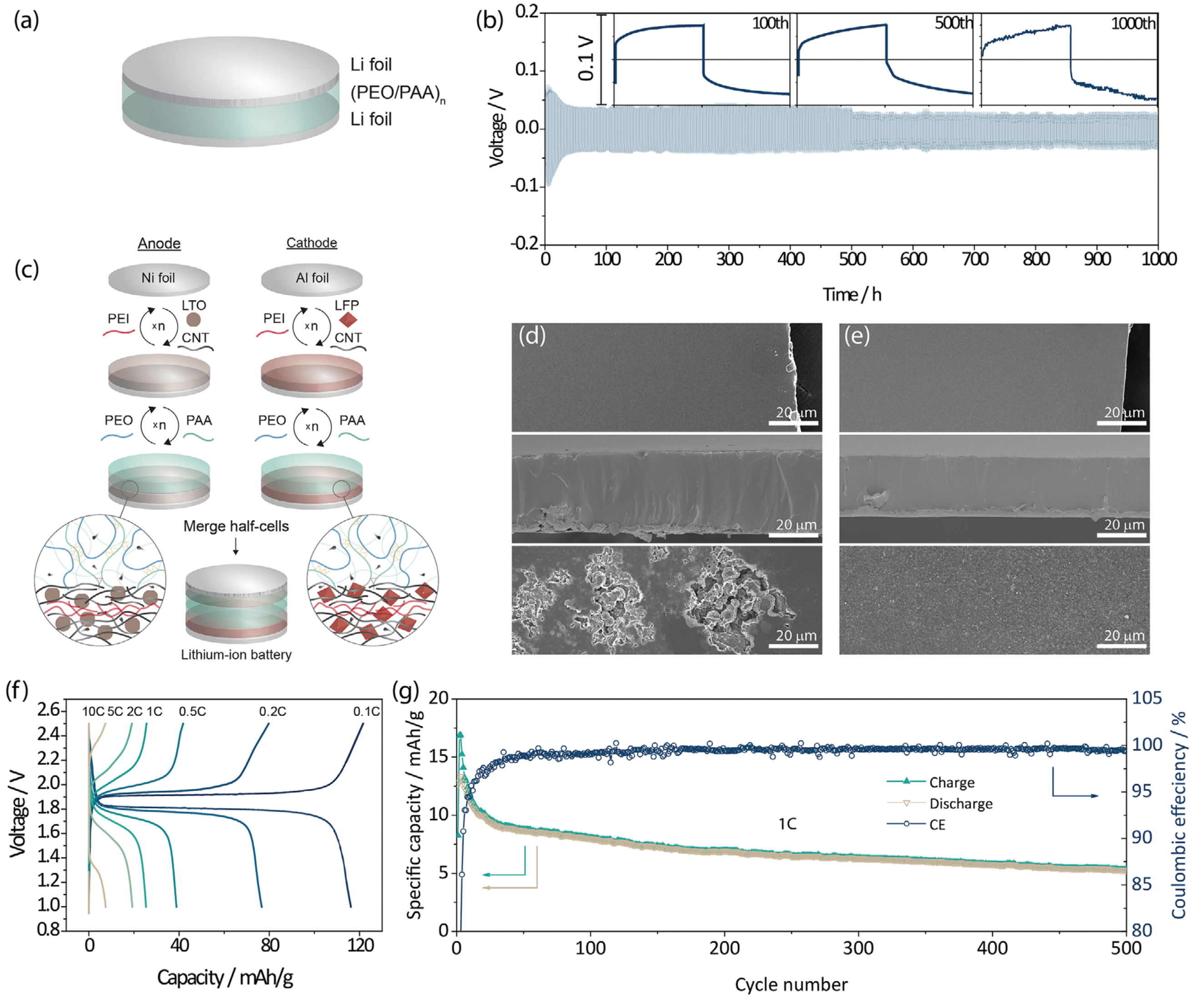

Figure 3. a) Schematic illustration showing the configuration of the symmetric Li cell; b) Li striping/plating test using the electrolyte soaked PEO/PAA240k thin film as the separator; c) schematic illustration showing the configuration of the all-LbL-assembled LIB; d) top-view, cross-sectional, and bottom-view SEM images of all-LbL-assembled LFP cathode; e) top-view, cross-sectional, and bottom-view SEM images of all-LbL-assembled LTO anode; f) charge/discharge profiles at different current density and g) cyclic stability of the all-LbL-assembled full-cell LIB.

0.5 M $CaCl_2$, and 0.95 ± 0.01 mS cm^{-1} for 1× PBS buffer. We fabricated interdigitated electrodes from carbon nanotube to form a symmetric micro supercapacitor device. At ambient RH, the PEO/PAA thin film had a sticky surface that could be used to transfer the interdigitated micro electrodes onto the free-standing (PEO/PAA) film which acted as a self-supported gel electrolyte with the electronic device mounted on top. CVs showed a typical double-layer capacitive behavior for the device in Figure 4b. Figure 4c shows high capacity retention of 2.0 mF cm^{-2} at 100 mV s^{-1}, compared to 3.9 mF cm^{-2} at 5 mV s^{-1}, determined by CV, which indicated good rate capability facilitated by the high ionic conductivity of the thin-film gel electrolyte.

The free-standing PEO/PAA films also allowed assembly of multi-layer electrochromic devices. The films serve as a transparent solid electrolyte. As shown in Figure 4d, we laminated PEA/PAA onto a patterned conducting polymer poly(3,4-ethylenedioxythiophene) (PEDOT) to form an electrochromic display pixels in a matrix. The PEDOT pixels were printed from solution onto PET substrate and further patterned with a plotter-cutter. In this structure, the counter electrodes were on the sides of the active pixel and the ions were transported laterally through the membrane. When applying a voltage of 1 V, the PEDOT pixels could reversibly switch their color due to electrochromism.

Similarly, we patterned PEDOT organic electrochemical transistor (OECT) on flexible substrates (Figure 4f). The gate and the channel were connected by simply pasting the PEO/PAA onto the device. After hydration with 1× PBS, the film allows efficient modulation of the gate on the channel conductance, as shown in Figure 4g. These simple demonstrations show that strong thin solid electrolyte films are suitable for fabricating flexible electronics for a variety of next-generation applications.

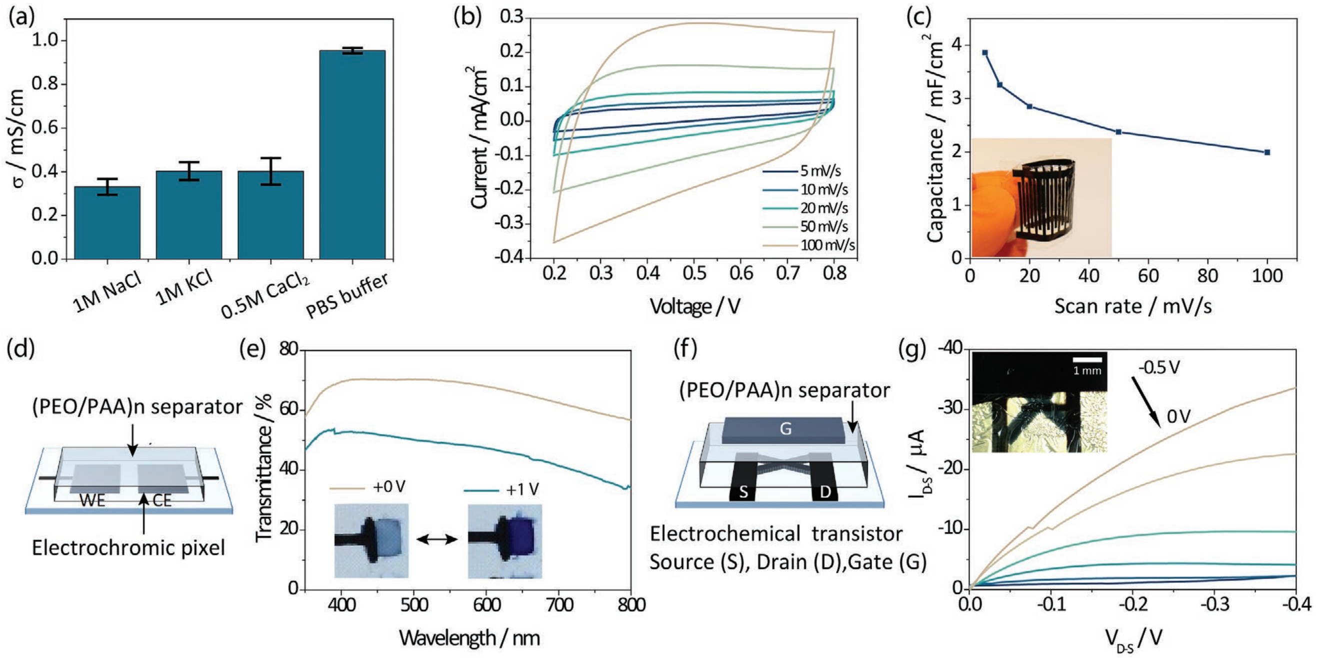

Figure 4. a) Ionic conductivity of the PEO/PAA films soaked by different aqueous solutions; b) CV curves and c) areal capacitance at various scan rates of the PEO/PAA240k thin film-borne supercapacitor; d) schematic illustration and photos showing the electrochromic behavior of the PEDOT device using PEO/PAA240k as the electrolyte; e) the corresponding transmittance spectra of the electrochromic device; f) schematic illustration and g) the corresponding steady state parameter of the PEDOT organic electrochemical transistor.

3. Conclusion

Using LbL self-assembly, we prepared thin film solid electrolytes, by using two common polymers PEO, and PAA. Here nonionic interactions between the PEO-PAA allowed for the LbL buildup, and we consequently heated the film to introduce covalent cross-links between PEO and PAA to strengthen the film, without decreasing its ionic conduction properties. These crosslinked (PEO/PAA) multilayers had three main advantages: i) They had a record high lithium ion conductivity of around $2.3 \pm 0.8 \times 10^{-4}$ S cm^{-1} at 30 °C, while at the same time being strong with a tensile strength of 3.7 ± 0.2 MPa. These are among the highest combined recorded values for multifunctional solid electrolytes. ii) They were self-healable, due to the nature of the reversible hydrogen bonds. More importantly when the thin films showed high stability in lithium cyclic plating/stripping test for at least 1000 cycles at a constant current of 0.05 mA cm^{-2} without any short circuit, it demonstrated that the self-healing film could suppress the growth of Li dendrites. iii) They could be used as separators to enable Li-ion batteries that were fully self-assembled from water. Self-assembled LFP/LTO full batteries delivered 116 mAh g^{-1} at 0.1 C. In addition, we could also use these strong free standing (PEO/PAA) solid electrolytes as substrates to assemble flexible supercapacitors and organic electronic transistors.

This method shows that LbL self-assembly allows the formation of nano composites of polymers with combined strength and ionic mobility by forming ordered structures that are not achievable by simple polymer mixing which leads to flocculation (Figure S9, Supporting Information). This system also opens up the possibility to incorporate inorganic compounds, such as clay as dendrites growth suppressing component[23] and Li-ion conducting ceramics for all solid state batteries.[24] By combining self-assembly of battery separators with self-assembly of the other components we are confident that this method will ultimately allow the formation of full 3D batteries.[25–27]

4. Experimental Section

Materials: PEO (4arm-PEG-NH_2, M_w: 40 kDa), PAA (M_w: 1200 Da, 8 kDa, 50 kDa, and 240 kDa), lithium hexafluorophosphate solution in ethylene carbonate and diethyl carbonate (1.0 M $LiPF_6$ in EC/DEC = 50/50 v/v), bis(trifluoromethane)sulfonimide lithium salt (LiTFSI, 99.95%), and PC (anhydrous, 99.7%) were products of Sigma Aldrich. Lithium foil (99.9%) was a product from Alfa Aesar. All chemicals were used as received. Water used in this work was ultrapure water obtained with a Milli-Q water purification system.

Characterizations: Scanning electron microscopic images were taken using a Hitachi S-4800 field-emission scanning electron microscope. The thermal analysis was carried out on a Mettler Toledo differential scanning calorimeter (Model DSC 1) using a nitrogen atmosphere. The ramp rate was 10 °C min^{-1}. Tensile tests were performed using an Instron 5944 universal testing machine with a strain rate of 40% min^{-1}. The pristine samples were conditioned in 50% RH at 25 °C overnight. The FTIR measurements were conducted with the aid of a Perkin Elmer Spectrum 100 FT-IR Spectrometer. XRD patterns were collected on a PANalytical X'Pert PRO powder diffractometer with a Cu-Kα source (wavelength 1.54178 Å).

The build-up of the layers were studiedusing a quartz crystal microbalance with dissipation (QCM-D, Model E4 from Q-Sense AB). The crystals for QCM-D measurement were AT-cut quartz crystal sensors with a silicon oxide layer (QSX 303). The solution of PEO and PAA were both 1 g L^{-1} in concentration at a pH of 2.4 and the rinsing water had the same pH. The adsorption and rising time was either 15 or 20 min, both of which were longer than the equilibrium time of the adsorption of each layer. The mass increase of each layer was calculated with QTool using a viscoelastic Voigt model, assuming the liquid density was 1 g mL^{-1} and the viscosity of the liquid was 1 g $m^{-1}\cdot s^{-1}$.

LbL Assembly: The PEO/PAA thin films were assembled on PP sheets (1 mm thick, from Sigma Aldrich) with the assistance of a dipping robot. Before assembly, the PP sheets were soaked in a PEI solution (60 kDa, 1 g L^{-1}, pH 7.5). For LbL assembly, the PEI-coated PP was alternatively dipped into the aqueous solution of PAA (1 g L^{-1}) and PEO (1 g L^{-1}) for 2 min, followed by 3 times of rinsing for 1 min each, until reaching the number of layers required. All the solutions and rinsing water were at pH 2.4. The films were further cross-linked at 120 °C overnight to induce the formation of covalent crosslinks.

Ionic Conductivity Measurement: The PEO/PAA thin films were soaked in 1 M $LiPF_6$ in EC/DEC (50/50 v/v) or in 1 M LiTFSI in PC for 24 h. Afterward, the PEO/PAA thin films were sandwiched between two stainless steel disks (SSDs) and packed coin cells (CR2032) inside an argon filled glovebox with oxygen and moisture level lower than 1 ppm. The ionic conductivity was measured with a BioLogic VSP potentiostat/galvanostat equipped with electrochemical impedance spectroscopy using a two-electrode connection. The frequency range was 1 MHz to 200 Hz and the amplitude was 10 mV around the open circuit voltage.

The aqueous ionic conductivity was measured with the thin films after being soaked in the corresponding solutions for 24 h. The soaked thin films were sandwiched between two SSDs for measurements.

Electrochemistry Tests: The CV, rate performance, and the first 500 cycles of Li^+ striping/plating tests were performed with a BioLogic VSP potentiostat/galvanostat using a two-electrode connection. The battery cycling measurements and the 501th–1000th cycles were conducted on a Land CT2001A battery testing system. 1 C charge/discharge rate was defined as 175 mAh g^{-1} for LTO and 170 mAh g^{-1} for LFP and the specific capacity of the half-cells was calculated based on the mass of the active materials. For the full cells, 1 C was defined as 140 mAh g^{-1} and calculated the specific capacity based on the mass of LTO. The capacity of the LFP cathode was excessive by 50%.

Organic Electrochemical Transistor: The OECT channel and gate was fabricated by filtering PEDOT microgel through wax-patterned filtration membrane. The electric contacts were assembled by aligning patterned carbon nanotubes onto the channel. The PEO/PAA film \was directly pasted onto the device. After hydration, the film bridged the gate and the channel with mobile ions. The measurements were performed on a Keithley 2401 and a Keithley 2410, controlled by Keithley Kickstart software.

Supporting Information

Supporting Information is available from the Wiley Online Library or from the author.

Acknowledgements

The authors acknowledge the European Research Council (Grant 715268), the Wenner-Gren Foundation, and Knut and Alice Wallenberg Foundation (through Wallenberg Wood Science Centre at KTH) for research funding. The authors thank Dr. Tobias Benselfelt for making the schematic illustrations.

Conflict of Interest

The authors declare no conflict of interest.

Data Availability Statement

The data that support the findings of this study are available from the corresponding author upon reasonable request.

Keywords

ionic conduction, lithium-ion batteries, mechanical strength, self-assembly

Received: February 16, 2021
Revised: April 28, 2021

---

[1] X. Cheng, J. Pan, Y. Zhao, M. Liao, H. Peng, *Adv. Energy Mater.* **2018**, *8*, 1702184.
[2] P. V. Wright, *Br. Polym. J.* **1975**, *7*, 319.
[3] Z. Xue, D. He, X. Xie, *J. Mater. Chem. A* **2015**, *3*, 19218.
[4] D. G. Mackanic, X. Yan, Q. Zhang, N. Matsuhisa, Z. Yu, Y. Jiang, T. Manika, J. Lopez, H. Yan, K. Liu, X. Chen, Y. Cui, Z. Bao, *Nat. Commun.* **2019**, *10*, 5384.
[5] J. Wan, J. Xie, X. Kong, Z. Liu, K. Liu, F. Shi, A. Pei, H. Chen, W. Chen, J. Chen, X. Zhang, L. Zong, J. Wang, L. Q. Chen, J. Qin, Y. Cui, *Nat. Nanotechnol.* **2019**, *14*, 705.
[6] C. A. C. Sequeira, D. M. F. Santos, *Polymer Electrolytes*, Woodhead Publishing, Cambridge **2010**.
[7] K. Xu, *Chem. Rev.* **2004**, *104*, 4303.
[8] A. Yuan, J. Zhao, *Electrochim. Acta* **2006**, *51*, 2454.
[9] F. X. Xiao, M. Pagliaro, Y. J. Xu, B. Liu, *Chem. Soc. Rev.* **2016**, *45*, 3088.
[10] D. M. DeLongchamp, P. T. Hammond, *Langmuir* **2004**, *20*, 5403.
[11] J. L. Lutkenhaus, K. D. Hrabak, K. McEnnis, P. T. Hammond, *J. Am. Chem. Soc.* **2005**, *127*, 17228.
[12] C. A. Nguyen, A. A. Argun, P. T. Hammond, X. Lu, P. S. Lee, *Chem. Mater.* **2011**, *23*, 2142.
[13] Z. Zou, Y. Li, Z. Lu, D. Wang, Y. Cui, B. Guo, Y. Li, X. Liang, J. Feng, H. Li, C. W. Nan, M. Armand, L. Chen, K. Xu, S. Shi, *Chem. Rev.* **2020**, *120*, 4169.
[14] H. G. M. Van de Steeg, M. A. Cohen Stuart, A. De Keizer, B. H. Bijsterbosch, *Langmuir* **1992**, *8*, 2538.
[15] Z. Wang, L. Ouyang, W. Tian, J. Erlandsson, A. Marais, K. Tybrandt, L. Wågberg, M. M. Hamedi, *Langmuir* **2019**, *35*, 10367.
[16] S. Xia, X. Wu, Z. Zhang, Y. Cui, W. Liu, *Chem* **2019**, *5*, 753.
[17] J. Lopez, Y. Sun, D. G. Mackanic, M. Lee, A. M. Foudeh, M. S. Song, Y. Cui, Z. Bao, *Adv. Mater.* **2018**, *30*, 1804142.
[18] S. Chen, Y. Zhao, J. Yang, L. Yao, X. Xu, *Ionics* **2017**, *23*, 2603.
[19] M. Echeverri, C. Hamad, T. Kyu, *Solid State Ionics* **2014**, *254*, 92.
[20] L. Porcarelli, C. Gerbaldi, F. Bella, J. R. Nair, *Sci. Rep.* **2016**, *6*, 19892.
[21] R. Bouchet, S. Maria, R. Meziane, A. Aboulaich, L. Lienafa, J.-P. Bonnet, T. N. T. Phan, D. Bertin, D. Gigmes, D. Devaux, R. Denoyel, M. Armand, *Nat. Mater.* **2013**, *12*, 452.
[22] X. Wang, F. Chen, G. M. A. Girard, H. Zhu, D. R. MacFarlane, D. Mecerreyes, M. Armand, P. C. Howlett, M. Forsyth, *Joule* **2019**, *3*, 2687.
[23] A. Mentbayeva, S. Sukhishvili, M. Naizakarayev, N. Batyrgali, Z. Seitzhan, Z. Bakenov, *Electrochim. Acta* **2021**, *366*, 137454.
[24] L. Chen, Y. Li, S.-P. Li, L.-Z. Fan, C.-W. Nan, J. B. Goodenough, *Nano Energy* **2018**, *46*, 176.
[25] Z. Wang, A. VahidMohammadi, L. Ouyang, J. Erlandsson, C.-W. Tai, L. Wågberg, M. M. Hamedi, *Small* **2020**, *17*, 2006434.
[26] G. Nystrom, A. Marais, E. Karabulut, L. Wagberg, Y. Cui, M. M. Hamedi, *Nat. Commun.* **2015**, *6*, 7259.
[27] J. W. Long, B. Dunn, D. R. Rolison, H. S. White, *Adv. Energy Mater.* **2020**, *10*, 2002457.